

Cosmic evolution of stellar quenching by AGN feedback: clues from the Horizon-AGN simulation

R. S. Beckmann^{1,*}, J. Devriendt^{1,2}, A. Slyz¹, S. Peirani^{3,4}, M. L. A. Richardson¹, Y. Dubois^{3,4}, C. Pichon^{3,4,5}, N. E. Chisari¹, S. Kaviraj⁶, C. Laigle¹, M. Volonteri^{3,4}

¹ *Sub-department of Astrophysics, University of Oxford, Keble Road, Oxford OX1 3RH, UK*

² *Observatoire de Lyon, UMR 5574, 9 avenue Charles Andre, F-69561, Saint Genis Laval, France*

³ *Sorbonne Universites, UPMC Univ Paris 06, UMR 7095, Institut d’Astrophysique de Paris, F-75005, Paris, France*

⁴ *CNRS, UMR 7095, Institut d’Astrophysique de Paris, 98bis Boulevard Arago, F-75014, Paris, France*

⁵ *Korea Institute for Advanced Study (KIAS), 85 Hoegiro, Dongdaemun-gu, Seoul, 02455, Republic of Korea*

⁶ *Centre for Astrophysics Research, University of Hertfordshire, College Lane, Hatfield, Herts, AL10 9AB*

30 January 2017

ABSTRACT

The observed massive end of the local galaxy stellar mass function is steeper than its predicted dark matter (DM) halo counterpart in the standard Λ CDM paradigm. We investigate how the effect of active galactic nuclei (AGN) feedback can account for such a reduction in the stellar content of massive galaxies, through an influence on the gas content of their interstellar (ISM) and circum-galactic medium (CGM). We isolate the impact of AGNs by comparing two simulations from the HORIZON suite, which are identical except that one includes super massive black holes (SMBH), and related feedback models. This allows us to cross-identify individual galaxies between these simulations and quantify the effect of AGN feedback on their properties, such as stellar mass and gas outflows. We find that the most massive galaxies ($M_* \geq 3 \times 10^{11} M_\odot$) are quenched to the extent that their stellar masses decrease by about 80% at $z = 0$. More generally, SMBHs affect their host halo through a combination of outflows that reduce their baryonic mass, particularly for galaxies in the mass range $10^9 M_\odot \leq M_* \leq 10^{11} M_\odot$, and a disruption of central gas inflows, which limits in-situ star formation, particularly massive galaxies with $M_* \approx 10^{11} M_\odot$. As a result of these processes, net gas inflows onto massive galaxies drop by up to 70%. Finally, we measure a redshift evolution in the stellar mass ratio of twin galaxies with and without AGN feedback, with galaxies of a given stellar mass showing stronger signs of quenching earlier on. This evolution is driven by a progressive flattening of the $M_{\text{SMBH}} - M_*$ relation for galaxies with $M_* \leq 10^{10} M_\odot$ as redshift decreases, which translates into smaller SMBHs being harboured by galaxies of any fixed stellar mass. This in turn indicates that stronger AGN feedback is operating at higher redshift.

Key words: galaxies: evolution - galaxies: high-redshift - galaxies: quasars: super-massive black holes - galaxies: star formation - galaxies: active - galaxies: nuclei - cosmology - methods: numerical

1 INTRODUCTION

It has long been known that the hierarchical structure formation paradigm implied by the cold dark matter model, while very successful overall, overproduces objects at the bright and faint end of the luminosity function (White & Frenk 1991; Kauffmann et al. 1993). Observations show much more

inefficient star formation in low and high mass halos, with a peak in efficiency at the luminosity turnover (Bernardi et al. 2013; Moustakas et al. 2013; Davidzon et al. 2017). To avoid the overcooling problem, and reproduce the observed luminosity function, an energetic feedback mechanism is required (Cole et al. 1994; Binney & Tabor 1995; Cattaneo 2001; Springel et al. 2005; Dubois et al. 2013). Several different avenues have been suggested to provide the necessary energy input and quench star formation, including the ex-

* Email: ricarda.beckmann@physics.ox.ac.uk

tragalactic UV background, supernova (SN) feedback and feedback due to active galactic nuclei (AGN).

Photoionisation by the extragalactic UV background and the first generations of stars suppresses gas accretion at high redshift, causing a number of smaller dark matter (DM) halos to remain devoid of gas (Gnedin 2000; Somerville 2002; Okamoto et al. 2008; Geen et al. 2013). While this mechanism provides a possible solution to the overabundance of very low mass ($\leq 10^8 M_\odot$) substructures in Milky-Way like halos, it has been shown to have little effect on more massive objects that collapse later (Efstathiou 2000; Governato et al. 2007).

On the other hand, SN feedback is widely believed to play an important part in quenching star formation in halos with masses below $10^{11} M_\odot$ (Dekel & Silk 1986; Benson et al. 2003; Hopkins et al. 2014). Their shallow potentials allow SN driven winds with velocities comparable to the escape velocity (Mac Low & Ferrara 1999; Christensen et al. 2016; Keller et al. 2015) to empty the host galaxy of a significant amount of gas, thereby efficiently suppressing star formation. However, even stellar feedback concentrated in intense, compact starbursts caused by major mergers or violent disc instabilities cannot quench massive galaxies (Dekel & Burkert 2014).

It has been suggested that star formation halts in massive objects due to a slowdown in cold flows at low redshift (Feldmann & Mayer 2014). However Mandelbaum et al. (2016) show that massive quiescent galaxies can have twice as much DM as star forming galaxies, indicating that cosmic inflows probably continue long after star formation has ceased. Furthermore, the slowdown in cold flows is expected to take place over Gyr timescales (Zolotov et al. 2015), which contradicts observational evidence that quenching of massive galaxies takes place on much shorter timescales (Barro et al. 2016; Tomczak et al. 2016). Therefore the reduction of star formation in massive galaxies is unlikely to occur solely because accretion is fading away.

Instead, AGN feedback could provide an effective route to quenching massive galaxies, as well as regulating the growth of supermassive black holes (SMBH) (Binney & Tabor 1995; Benson et al. 2003; Di Matteo et al. 2005; Bower et al. 2006; Croton et al. 2006; Sijacki et al. 2007; Cattaneo et al. 2009; Fabian 2012). There are two main mechanisms through which this could proceed. One possibility is that black holes and stars feed from the same cold gas supply until it is depleted by AGN feedback, at which point both processes come to a halt. Observations of galaxies that simultaneously harbour both an AGN and an active starburst provide evidence that supports this claim (Heckman & Kauffmann 2006; Nardini et al. 2008; Lutz et al. 2008). In this scenario, AGN feedback might even accelerate star formation by further compressing the cold gas of the galaxy, in a so called positive feedback mode (Silk 2005; Gaibler et al. 2012; Santini et al. 2012; Bieri et al. 2015). However, its main role is to prevent the gas heated/expelled by SN winds to be re-accreted at a later stage, alongside more pristine material. This is the so called maintenance mode, associated with powerful radio emission (Rafferty et al. 2006; Cattaneo & Teysier 2007).

Alternatively, AGN feedback could act directly on the gas content of the galaxy. It could expel the interstellar medium (ISM) out of galaxies in massive galactic winds,

and/or prevent star formation by directly heating the ISM gas (Springel et al. 2005; Di Matteo et al. 2005; Murray et al. 2005; Fabian et al. 2006). This view is supported by observational evidence of frequent and fast outflows in massive galaxies (Tremonti et al. 2007), able to drive a significant gas mass (Heckman et al. 2000; Veilleux et al. 2005; Weiner et al. 2009; Sturm et al. 2011) using only 5 – 10% of accretion power (Moe et al. 2009; Saez et al. 2009; Dunn et al. 2010). Whilst such outflows are common in maintenance mode radio quasars (De Kool et al. 2001; Arav et al. 2001; Reeves et al. 2003; Chartas et al. 2007; Dunn et al. 2010; Moe et al. 2009), careful analysis of higher redshift objects provides evidence that quasars can also launch powerful energy driven winds and thus cause a rapid star formation decline (Maiolino et al. 2012; Page et al. 2012; Farrah et al. 2012; Cicone et al. 2014; Costa et al. 2015; Williams et al. 2016). Both modes of AGN feedback can reproduce the observed correlations between host galaxy and BH properties (Ferrarese & Merritt 2000; Gebhardt et al. 2000), as shown by e.g. Di Matteo et al. (2008); Booth & Schaye (2009); Dubois et al. (2012); Sijacki et al. (2015); Volonteri et al. (2016). However, the timescale over which quenching takes place is still a matter of debate, with evidence existing for both rapid quenching (Thomas et al. 2005) and much slower processes (Quintero et al. 2004). The timescales are probably dependent on galaxy type (Schawinski et al. 2014).

In this work we use state-of-the-art cosmological simulations to investigate when and how AGN feedback affects its host galaxy. We isolate the impact of such feedback on stellar masses and large scale gas flows by comparing the evolution of a statistically representative sample of individual objects, identifying matching galaxies in two simulations, HORIZON-AGN (H-AGN) and HORIZON-noAGN (H-noAGN). As their names indicate, these simulations are identical in all aspects except one is run with and the other without AGN feedback. Following the evolution of twinned galaxies from redshift $z = 5$ down to $z = 0$ allows us to determine the epoch of quenching, and identify ensuing changes in the stellar masses of affected galaxies.

The paper is structured as follows: Section 2 briefly introduces the HORIZON simulation suite and Section 3 explains the procedure used to identify pairs of corresponding objects across both simulations. Section 4 presents the effect of AGN feedback on galaxy stellar masses throughout cosmic time and Section 5 determines the causes for the measured quenching by studying the evolution of the black hole population, the gas content of halos and galaxies and gas inflow/outflow rates. Section 6 summarises and discusses our results.

2 THE SIMULATIONS

This paper presents a comparative analysis of two simulations: HORIZON-AGN (H-AGN) and HORIZON-noAGN (H-noAGN). Both simulations are run from identical initial conditions and share the same technical specifications and implementations of physics. The only difference is that HORIZON-AGN also includes a sub-grid modelling of SMBHs and the associated AGN feedback (see Section 2.5) whereas H-noAGN does not. More details can be found in Dubois et al. (2014).

2.1 Cosmology and initial conditions

Both simulations were run with RAMSES (Teyssier 2002), an adaptive mesh refinement code, using a second-order unsplit Godunov scheme to solve the Euler equations. A HLLC Riemann solver with a MinMod Total Variation Diminishing scheme was used to reconstruct interpolated variables. Initial conditions were produced using MP-GRAFIC (Prunet et al. 2008) and both simulations were carried out until $z = 0.0$.

The initial conditions setup is a standard Λ CDM cosmology consistent with the WMAP-7 data (Komatsu et al. 2011), with $\Omega_m = 0.272$, dark energy density $\Omega_\Lambda = 0.728$, baryon density $\Omega_b = 0.045$, Hubble constant $H_0 = 70.4 \text{ km s}^{-1} \text{ Mpc}^{-1}$, amplitude of the matter power spectrum $\sigma_8 = 0.81$, and power-law index of the primordial power spectrum $n_s = 0.967$.

The simulated cube of $L_{\text{box}} = 100 \text{ Mpc/h}$ on a side is initially refined uniformly down to physical $\Delta x = 1 \text{ kpc}$, which requires a root grid with 1024^3 cells at $z \simeq 100$. To keep the size of the smallest cells approximately constant in physical units, a new level of refinement is adaptively added to the grid every time the expansion factor doubles. These extra refinement levels are triggered using a quasi-Lagrangian criterion: a grid cell is split into 8 if its Dark Matter (DM) or baryonic mass exceeds 8 times the initial DM or baryonic mass respectively.

There are a total of 1024^3 DM particles in each simulation, leading to a DM mass resolution of $8 \times 10^7 M_\odot$. All collisionless particles, i.e. DM and stars, are evolved using a multi-grid Poisson solver with a cloud-in-cell interpolation to assign particles to grid cells.

2.2 Cooling and heating

The gas is allowed to cool down to 10^4 K using H, He and atomic metal cooling, following Sutherland & Dopita (1993) and accounting for photon heating by a uniform UV background (Haardt & Madau 1996) from $z_{\text{reion}} = 10$ onwards. The ratio between elements is assumed to be solar in these cooling/heating calculations. The gas follows a mono-atomic equation of state, with adiabatic index $\gamma = 5/3$.

2.3 Stars and Supernovae

Star formation is modelled using a Kennicutt–Schmidt law $\dot{\rho}_* = \epsilon_* \rho / t_{\text{ff}}$, where $\dot{\rho}_*$ is the star formation rate density, $\epsilon_* = 0.02$ the (constant) star formation efficiency (Kennicutt, Jr. 1998; Krumholz & Tan 2007), ρ the gas density and t_{ff} the local free fall time of the gas. Stars form when the gas number density exceeds $\rho_0 / (\mu m_{\text{H}}) = 0.1 \text{ H/cm}^3$ where m_{H} is the mass of a hydrogen atom and μ the mean molecular weight, and star particles are generated according to a Poisson random process (Rasera & Teyssier 2006; Dubois & Teyssier 2008) with a stellar mass resolution of $M_* = \rho_0 \Delta x^3 \simeq 2 \times 10^6 M_\odot$. To avoid numerical fragmentation, and mimic the effect of stellar heating by young stars, a polytropic equation of state, $T = T_0 (\rho / \rho_0)^{\kappa-1}$, is used for gas above the star formation density threshold, with $\kappa = 4/3$.

For stellar feedback, a Salpeter initial mass function (IMF) (Salpeter 1954) is assumed, with low and high mass

cutoffs of $0.1 M_\odot$ and $100 M_\odot$ respectively. In an effort to account for stellar feedback as comprehensively as possible, the (sub-grid) model implemented in this work includes stellar winds, Type II and Type Ia supernovae. Mechanical feedback energies from Type II supernovae and stellar winds are computed using STARBURST99 (Leitherer et al. 2010, 1999). Specifically, we use a Padova model (Girardi et al. 2000) with thermally pulsating asymptotic branch stars (Vassiliadis & Wood 1993), and stellar winds are calculated as in Leitherer et al. (1992). The frequency of Type I SN is estimated from Matteucci & Greggio (1986), assuming a binary fraction of 5%. To reduce computational costs, stellar feedback is modelled as a source of kinetic energy during the first 50 Myr of the lifetime of star particles, and as a heat source after that. On top of energy, mass and metals injected into the interstellar medium (ISM) by stellar feedback, we also keep track a variety of chemical elements (O, Fe, C, N, Mg, Si) synthesised in stars, with stellar yields estimated according to the W7 model of Nomoto et al. (2007). More detailed discussions of the stellar feedback model used can be found in Dubois & Teyssier (2008); Kimm et al. (2015); Rosdahl et al. (2017).

2.4 SMBH formation and accretion

In H-AGN, black holes are seeded with an initial mass of $10^5 M_\odot$ in dense, star-forming regions, i.e. when a gas cell exceeds $\rho > \rho_0$ and is Jeans unstable, provided such regions are located more than 50 kpc away from a pre-existing black hole (Dubois et al. 2010). These black holes subsequently accrete gas at the Bondi-Hoyle-Lyttleton rate:

$$\dot{M}_{\text{BH}} = \frac{4\pi\alpha G^2 M_{\text{BH}}^2 \bar{\rho}}{(\bar{c}_s^2 + \bar{u}^2)^{3/2}}, \quad (1)$$

where M_{BH} is the black hole mass, $\bar{\rho}$ is the average gas density, \bar{c}_s is the average sound speed, and \bar{u} is the average gas velocity relative to the BH. To counteract resolution effects that make it difficult to capture cold, dense regions of the ISM, a boost factor α is used, following Booth & Schaye (2009):

$$\alpha = \begin{cases} (\rho/\rho_0)^2 & \text{if } \rho > \rho_0 \\ 1 & \text{otherwise} \end{cases} \quad (2)$$

Accretion is capped at the Eddington rate $\dot{M}_{\text{Edd}} = 4\pi G M_{\text{BH}} m_p / (\epsilon_r \sigma_{\text{T}} c)$ where σ_{T} is the Thomson cross section, m_p is the proton mass, and c is the speed of light. A standard radiative efficiency, typical of a Shakura–Sunyaev accretion disc around the BHs, of $\epsilon_r = 0.1$ is assumed (Shakura & Sunyaev 1973).

BHs are also allowed to merge with one another when they are closer than 4kpc, and their relative velocity is smaller than the escape velocity of the binary.

2.5 AGN feedback

Two modes of AGN feedback are implemented in H-AGN, depending on the instantaneous accretion rate of the SMBH: the so-called radio and quasar modes.

At high accretion rates, i.e. for Eddington ratios $\chi = \dot{M}_{\text{BH}} / \dot{M}_{\text{Edd}} > 0.01$, the quasar mode deposits thermal energy isotropically into a sphere of radius Δx centred on the

Number of twins per mass category			
z	Small	Medium	Large
0.5	11,196	57,734	1,410
1	13,393	60,547	773
3	11,823	19,855	7
5	2,949	1,626	0

Table 1. Number of galaxy twins in each sub-sample, at the range of redshifts presented here.

BH. This energy is deposited with an efficiency of $\epsilon_f = 0.15$ at a rate of

$$\dot{E}_{\text{AGN}} = \epsilon_f \epsilon_r \dot{M}_{\text{BH}} c^2. \quad (3)$$

The radio mode takes over at low accretion rates, $\chi = \dot{M}_{\text{BH}}/\dot{M}_{\text{Edd}} \leq 0.01$, and deposits kinetic energy into bipolar outflows with jet/wind velocities of 10^4 km/s, along an axis aligned with the angular momentum of the accreted material, following the model of [Omma et al. \(2004\)](#). The total rate of energy deposited is given by the previous equation for \dot{E}_{AGN} , albeit using a higher efficiency of $\epsilon_f = 1$ (see [Dubois et al. \(2010\)](#) for detail).

The radiative efficiencies of the two AGN feedback modes were chosen to reproduce the scaling relations between BH mass and galactic properties in the local universe, $M_{\text{SMBH}} - M_*$ and $M_{\text{SMBH}} - \sigma_*$ ([Dubois et al. 2012](#)). Note that these two parameters are the only ones which are tuned in the HORIZON simulations, in the sense that the other parameters (associated with the sub-grid models of star formation and stellar feedback) were not allowed to vary in order to obtain a better match to bulk galaxy properties. For instance, even though our star formation efficiency choice ensures that galaxies will fall on the Kennicutt observational law by construction, it does not automatically guarantee that they will have the correct stellar/gas mass and/or size at any epoch.

2.6 Mass categories for galaxies

For the purpose of facilitating the presentation of our results, we split our sample of galaxy twins into three sub-samples, distinguished by the stellar mass of the H-AGN galaxy. We define *small* galaxies as twins with stellar masses $M_*^{\text{H-AGN}} < 10^9 M_\odot$ in H-AGN, *medium* galaxies as those with $10^9 M_\odot \leq M_*^{\text{H-AGN}} \leq 10^{10} M_\odot$ and *large* galaxies as those with $M_*^{\text{H-AGN}} > 10^{10} M_\odot$. See Table 1 for the number of twins in each mass category. As a visual guidance, these mass categories will be annotated by solid vertical lines on all relevant plots.

3 HALO MATCHING ACROSS SIMULATIONS

3.1 The twinning procedure

Having two simulations based on identical initial conditions allows the identification of corresponding objects within both simulations, a procedure here referred to as ‘‘twinning’’ (see also e.g. [Geen et al. 2013](#)). A pair of corresponding halos is called a twin, and identifies two objects that have grown from the same overdensity in the initial conditions.

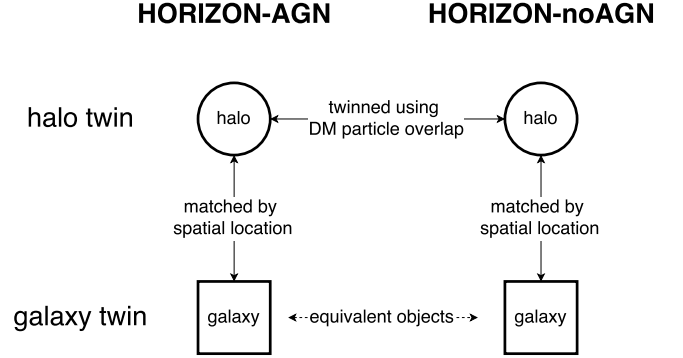


Figure 1. To twin galaxies across H-AGN and H-noAGN, DM halos are first identified in each simulation, and halos that show a 75% or more overlap in the identities of their DM particles are twinned. Galaxies are then associated with a unique host halo in each simulation, based on how close they are to the centre of the halo (see text for detail). Galaxies associated with halo twins are considered galaxy twins.

The objects can either be halos, for halo twins, or galaxies, for galaxy twins. If all the algorithms implemented to describe physical processes were identical in both simulations, the twins would be identical except for minor differences introduced by the stochastic nature of the star formation algorithm. However, such seemingly innocuous differences would already prevent us from directly twinning galaxies. We therefore employ the more general method of [Peirani et al. \(2016\)](#) to perform this task, which is summarised in Fig. 1. Only DM halos are twinned directly; to create galaxy twins, each galaxy is first associated with its host halo, then with the host halo twin in the other simulation and finally with the galaxy hosted by this twin halo.

More specifically, as both simulations start from identical initial conditions, with uniquely identified DM particles in identical positions, we can identify which of these particles cluster to form gravitationally bound halos as the runs proceed. Halos that grew from the same initial overdensities in both simulations should contain a large fraction of DM particles with identical identities at any time. In practice, for two DM halos to be twinned, we require that at least 75% of the DM particles present in a halo in H-AGN are also present in the H-noAGN halo. Note that in some cases, this choice will lead to a single halo in H-noAGN being associated with several halos in H-AGN, as halos mergers lead to the formation of sub-halos which are not necessarily disrupted at the same time in both simulations. In these cases, the object with the most similar mass is chosen as the twin halo, and the other matches are discarded.

Star particles stochastically form over the course of a simulation and their identifiers therefore reflect the detailed star formation history of that precise simulation, so it is not possible to identify galaxy twins directly through their star particle identities as is done for DM halos. Instead, galaxies are considered to be twins if they are located within DM halo twins (see Fig. 1). We begin by assigning a host halo to each galaxy if its centre is located within a distance $R_{\text{host}} = 0.05 \times R_{\text{vir}}$ of the centre of the halo. In case a halo contains more than one galaxy in its central region, we select the

Number of halos				
z	$N^{\text{H-AGN}}$	$N^{\text{H-noAGN}}$	$N^{\text{H-noAGN}}/N^{\text{H-AGN}}$	N_{twinned}
0.5	90,660	88,249	0.97	79,218
1	89,930	88,488	1.02	83,176
3	53,363	53,551	1.00	53,357
5	16,042	16,065	1.00	15,818

Number of galaxies				
z	$N^{\text{H-AGN}}$	$N^{\text{H-noAGN}}$	$N^{\text{H-noAGN}}/N^{\text{H-AGN}}$	N_{twinned}
0.5	80,740	79,930	0.99	70,340
1	80,588	82,238	1.02	74,713
3	34,128	47,428	1.39	31,685
5	6,255	7,757	1.24	4,575

Table 2. Number of galaxies, halos and twins identified in H-AGN and H-noAGN. The sample includes all halos resolved by 500 DM particles, and all galaxies resolved by at least 50 star particles, hosted in those halos.

most massive one as being hosted by this halo and discard other matching objects.

3.2 Matched fractions

As we are interested in the most massive objects, the full sample considered here includes all halos resolved by at least 500 DM particles, and all galaxies hosted in these halos that contain at least 50 star particles. Across all redshifts, H-AGN and H-noAGN contain a comparable number of both galaxies and halos (see Table 2). For this reason, the following analysis considers the H-AGN sample as the reference to analyse the effectiveness of the twinning algorithm.

Fig. 2 shows that at high redshift, over 98% of halos present in H-AGN, corresponding to 15,818 out of 16,042 at redshift $z = 5$, are twinned successfully, with an even distribution across all mass bins. At lower redshift, the fraction of matched objects decreases as the more and more different merger histories in the two simulations introduce larger discrepancies between individual objects. This fraction also decreases with halo mass, as halos with smaller particle numbers are more sensitive to these merger history changes. However, with 79,218 halos twinned at redshift $z = 0.5$ out of a sample of 90,660, i.e. an average matched fraction of 87%, the resulting sample remains statistically representative.

The overall rates for matched galaxies are much lower than for halos, as they require three steps to establish the link (galaxy to host halo, host halo to host halo twin, host halo twin to galaxy twin, see Fig. 1), with a number of objects dropping out of the sample at each step. Identifying a galaxy with its host halo can be challenging, especially in dense environments and at high redshift where interactions are more common. For example, increasing the size of the region within which a galaxy is associated with its host halo, R_{host} , from $R_{\text{host}} = 0.05 \times R_{\text{vir}}$ to $R_{\text{host}} = 0.10 \times R_{\text{vir}}$, significantly increases the fraction of matched galaxies for high redshift (see Chisari et al, 2017, in prep). More specifically, for redshift $z = 3$, the total number of galaxies, at any resolution, identified with a host halo, would rise from 67,572 to 94,942, out of 109,960 galaxies in total, which rep-

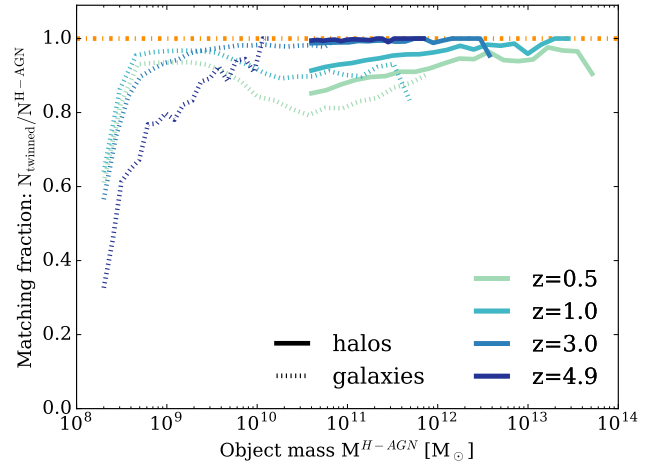


Figure 2. Fractions of matched halos (solid lines) and galaxies (dashed lines) in the H-AGN and H-noAGN simulations. The dashed-dotted line represents the ideal case where all objects in H-AGN are uniquely associated with a corresponding object in H-noAGN. More than 86% of halos are twinned, but galaxy twinning is less efficient, particularly at masses below $M_*^{\text{H-AGN}} = 10^9 M_\odot$ or at redshift $z \leq 1$.

resents an increase in matched fraction from 61% to 86%. However, we have checked that relaxing our twinning criteria does not significantly alter the quantitative results presented in this work. In other words, the galaxy sample, defined as described in this section, is statistically robust enough, at all redshifts and galaxy masses, for us to draw conclusions about the impact of AGN feedback in the H-AGN simulation.

3.3 The effect of AGN feedback on halos

Fig. 3 shows that no matter the redshift, the DM halo mass functions (HMF) for H-AGN and H-noAGN are so similar that they are indistinguishable on the plot. Directly comparing the DM masses of halo twins (See Fig. 4) shows that halos with masses below $M_{\text{vir}}^{\text{H-AGN}} < 10^{11} M_\odot$ have identical masses in both simulations, at all redshifts. The small spread in masses is mainly caused by variations in shape, which the structure finding algorithm translates into a small variation in virial mass. At redshifts of $z = 1$ and below, halos with masses above $M_{\text{vir}}^{\text{H-AGN}} > 10^{11} M_\odot$ can have a dark matter mass up to 5% percent lower in H-AGN. This is due to the fact that in the presence of AGN feedback, the baryon content of these massive halos is strongly reduced (see Section 5), which translates into a reduced total halo mass, as the reduced gravitational pull slows down the cosmic inflow rate. As the halos in H-AGN systematically exhibit lower masses, it makes sense to require, as we do, that 75% of DM particles from H-AGN be present in the H-noAGN halo, and not the reverse. A more detailed analysis as to how AGN feedback affects the inner structure of DM halos is carried out in Peirani et al. (2016).

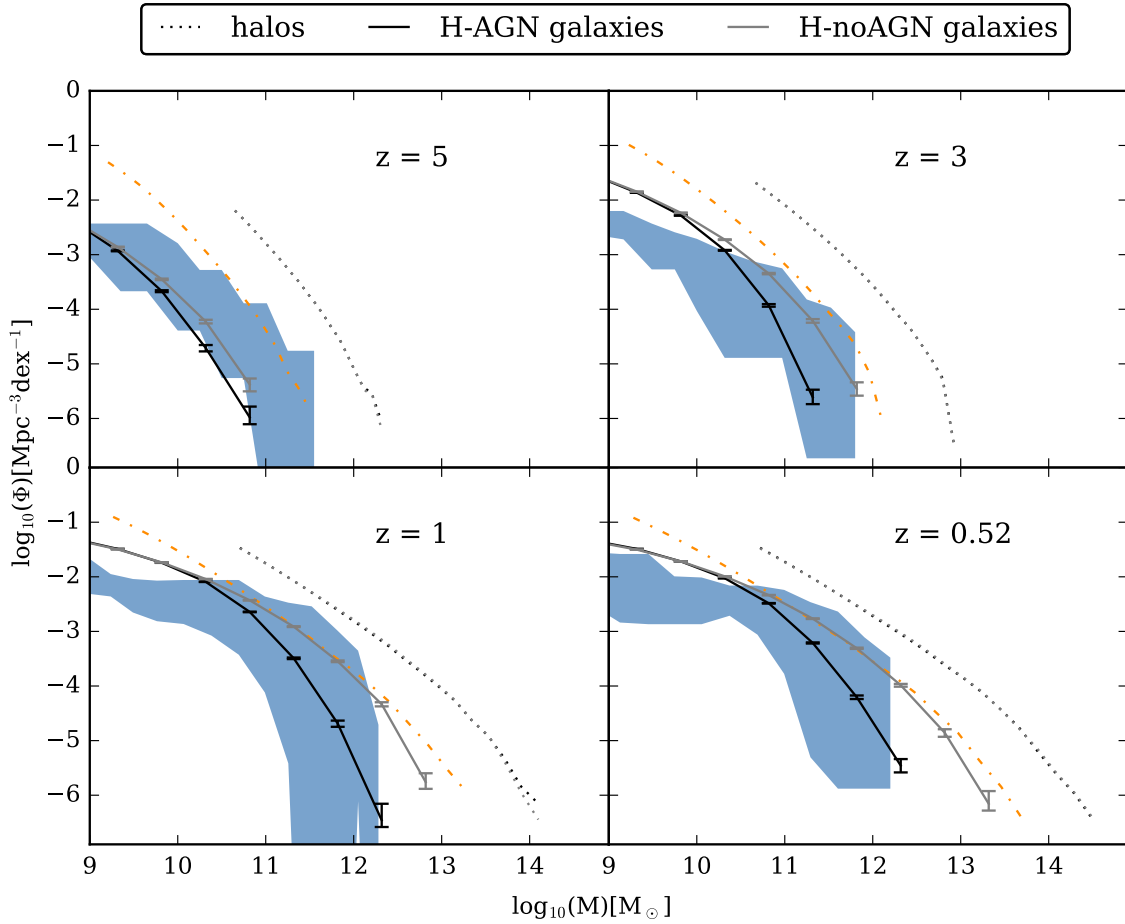


Figure 3. DM halo mass functions (HMF) (dotted) and corresponding galaxy stellar mass functions (GSMF) (solid) for H-AGN (black) and H-noAGN (light grey). We also plot the GSMF expected if all the baryons within halos (using a fraction of 16.5% of the total mass) are converted into stars (dot-dashed line), and combined observations from [Bielby et al. \(2014\)](#); [Daddi et al. \(2002\)](#); [Moustakas et al. \(2013\)](#); [Tomczak et al. \(2014\)](#); [González et al. \(2011\)](#); [Song et al. \(2016\)](#) as the shaded area. Errorbars on the simulation mass functions are Poisson, with those on the HMF not plotted as they are even smaller than the GSMF ones in the mass range where they overlap. Both HMF for H-AGN and H-noAGN are plotted, but are so similar as to be indistinguishable. At redshifts $z \leq 3$, the GSMFs from H-AGN show good agreement with observations above stellar masses of $M_* > 5 \times 10^{10} M_\odot$. At $z = 5$, the H-AGN simulation tends to underproduce galaxies more massive than $M_* > 10^{10} M_\odot$.

4 AGN FEEDBACK & STELLAR MASS

4.1 The galaxy stellar mass function

Comparing the galaxy population in H-AGN and H-noAGN at the various redshifts presented in this work shows that AGN feedback is instrumental in bringing the massive end of the GSMF in agreement with observations. As Fig. 3 demonstrates, AGN feedback is able to suppress star formation in galaxies with masses $M_* \geq 5 \times 10^{10} M_\odot$ at $z = 3$, allowing the simulation to correctly capture the knee and massive end of the GSMF. It is important to note that H-AGN was *not* tuned to reproduce this result. As previously mentioned, the only tuning done on global galaxy properties in the simulation involves the radiative efficiency of the AGN feedback modes, which were set to reproduce the local $M_{\text{SMBH}} - M_*$ and $M_{\text{SMBH}} - \sigma_*$ relations.

In the absence of AGN feedback, the GSMF in H-noAGN agrees well with predictions that the uniform baryon mass fraction of $\Omega_b/\Omega_m = 0.165$ (dotted-dashed lines, [Komatsu et al. 2011](#)) is entirely converted into stars in the galaxy mass range $5 \times 10^{10} M_\odot < M_* < 10^{12} M_\odot$ by $z = 1$. For galaxies with masses $M_* \geq 5 \times 10^{12} M_\odot$, a discrepancy between the GSMF in the absence of feedback (solid grey line) and expectation values from the cold dark matter model (dotted line) starts to appear because gas cooling times in host halos harbouring such massive galaxies become comparable to the Hubble time when the halos assemble, so not all the baryons enclosed have yet been able to cool and form stars. Cooling is further hampered by the fact that in the absence of AGN feedback, heavy elements do not get distributed effectively throughout the halo but remain close to the central galaxy.

The simulations systematically overproduce the num-

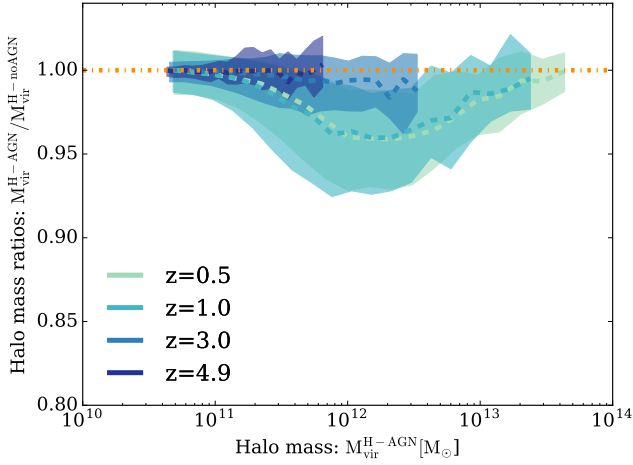


Figure 4. Twinned halo DM mass ratios in H-AGN and H-noAGN at different redshifts, with quartile error regions around the median (shaded region). Note that the median twin halo with $M_{\text{vir}}^{\text{H-AGN}} < 10^{11} M_{\odot}$ has an identical DM mass with and without AGN feedback, whatever the redshift. Median intermediate mass halos $2 \times 10^{11} M_{\odot} < M_{\text{vir}}^{\text{H-AGN}} < 2 \times 10^{13} M_{\odot}$ see their virial mass reduced by up to 5% depending on mass and redshift.

ber of galaxies with masses below $M_{*} \leq 5 \times 10^{10} M_{\odot}$ and $z \leq 3$. This is partly caused by the fact that observed mass functions are derived from magnitude-limited data, whereas the GSMF presented here for H-AGN and H-noAGN are raw stellar masses extracted from the simulation, with no completeness, surface brightness or luminosity cut applied. Indeed, comparing the GSMFs presented in Fig. 3 to those plotted in Fig. 7 of Kaviraj et al. (2016), which are based on the *same* simulation, H-AGN, but include a magnitude cut to match observations, one realises that the effective number of galaxies with masses $M_{*} = 10^9 M_{\odot}$ is reduced by about 0.5 dex at any redshift, whilst galaxies of mass $M_{*} \geq 5 \times 10^{10} M_{\odot}$ are completely unaffected. This considerably flattens the simulated GSMFs at the faint end, bringing them in much better agreement with the data. The remaining discrepancy can probably be attributed to the implementation of a less energetic feedback model, as well as to resolution effects (Kaviraj et al. 2016)¹. However, as AGN feedback, through the comparison of H-AGN and H-noAGN, is measured to have no effect on the low mass end of the GSMFs (as clearly visible in Fig. 3), and the issues discussed above are present in both simulations, they likely have a very limited impact on the work presented here. Still, any of our results for galaxies with a mass below $M_{*} \leq 5 \times 10^{10} M_{\odot}$ have to be examined bearing these caveats in mind.

Finally, both simulations systematically underproduce massive ($M_{*} \geq 5 \times 10^{10} M_{\odot}$) galaxies at redshift $z \geq 5$ (Fig. 3 top left panel). Given that the HMF multiplied by the universal baryon fraction (dot-dashed curve on the figure) seems to describe the observed data fairly well for galaxies in this mass range, this suggests that our inability to resolve

¹ A stronger SN feedback is likely to affect black hole masses as well Dubois et al. (2015); Habouzit et al. (2016).

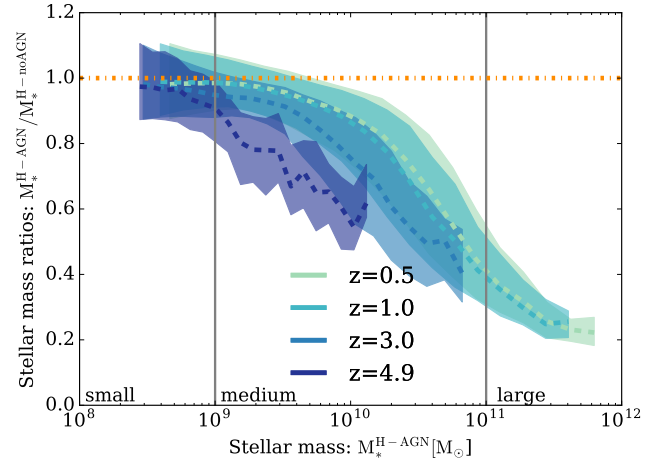


Figure 5. Quenching² fractions, i.e. stellar mass ratios of twinned galaxies in H-AGN and H-noAGN. The twins are mass binned by stellar mass in H-AGN, $M_{*}^{\text{H-AGN}}$, with the median value (dashed lines) and quartile error ranges (shaded region) plotted for each bin. If AGN feedback had no effect, the quenching fraction would lie on the horizontal dotted line, which denotes twin galaxies having identical mass. Note the non-linear evolution of the quenching fraction with galaxy mass, with small galaxies ($M_{*}^{\text{H-AGN}} < 10^9 M_{\odot}$) barely affected, and large galaxies ($M_{*}^{\text{H-AGN}} > 10^{11} M_{\odot}$) being most strongly quenched. This plot also shows a redshift evolution, with smaller galaxies more affected at higher redshift.

the progenitors of halos early enough leads to star formation being artificially postponed. Obviously, since the gas content of these halos is still correctly estimated, galaxies will eventually catch up: their star formation rate will be slightly higher than expected, as long as more gas is present. However, at high redshift, galaxy star formation timescales cannot be considered small in comparison to the time elapsed since their host halo formed, so their stellar masses can be significantly underestimated. Note that this resolution effect has completely vanished, at least for massive galaxies, by $z = 3$. Moreover, as this issue affects H-AGN and H-noAGN in the same way, it cancels out in the comparative analysis of the two simulations that we perform in this work.

4.2 Quenching²

Instead of having to rely on statistical averages, such as those presented in the mass functions in Fig. 3, the twinning procedure described in Section 3 allows for a direct comparison of the stellar masses of each individual galaxy, with and without AGN feedback. Fig. 5 shows the results of this comparison for a range of redshifts. As expected from

² For the purpose of this paper, “quenching” refers to any reduction in galaxy star formation rates (SFR) when AGN feedback is included, compared to the case without it, not just a SFR of $\dot{M}_{*} < 2 \times 10^{-11} M_{\odot}/\text{yr}$, as defined in Franx et al. (2008). Likewise, the “quenching fraction” refers to the stellar mass ratio of galaxy twins between the cases with and without AGN feedback, i.e. $M_{*}^{\text{H-AGN}}/M_{*}^{\text{H-noAGN}}$.

the local GSMF in Fig. 3, the most massive galaxies are the most strongly quenched at all redshifts (Fig. 5). However the amount of quenching does not vary linearly with galaxy mass, with the function tailing off for both strongly quenched large galaxies, and barely affected small galaxies.

We also measure a redshift dependence in the maximum amount of quenching observed, ranging from 40% for galaxies with stellar masses in H-AGN of $M_*^{\text{H-AGN}} > 10^{10} M_\odot$ at redshift $z = 5$, up to a maximum of over 80% for the largest galaxies at redshift $z = 0.5$, suggesting that galaxy quenching is a continuous process active throughout the merging history of galaxies. In general, the shape of the distribution is driven by small galaxies that show little influence of AGN feedback at any redshift, and a tailing off at the massive end. Large galaxies appear to converge to a constant quenching fraction $M_*^{\text{H-AGN}}/M_*^{\text{H-noAGN}} = 0.2$, as they grow from $M_* = 10^{11} M_\odot$ to $M_* = 10^{12} M_\odot$ both in H-AGN and H-noAGN. This is not due to any fundamental change in the impact of AGN feedback for galaxies with stellar masses above $M_* > 10^{11} M_\odot$ but rather reflects the fact that, even in the absence of AGN feedback, the GSMF in H-noAGN steepens due to long cooling times for massive objects (see Fig. 3 and Section 4.1) which lead to reduced star formation rates. Therefore, the constant quenching fraction for large galaxies is not driven by less effective AGN feedback, but rather by less effective cooling for galaxies in the absence of feedback. Note that this is not a selection effect either, as no mass ratio cut was applied to our galaxy sample.

Particularly noticeable for redshifts above $z > 3$, the minimum mass to experience quenching decreases with redshift: a typical $10^9 M_\odot$ galaxy at redshift $z = 5$ already has its stellar mass quenched by 10%, whereas a $10^9 M_\odot$ galaxy at redshift $z = 1$ shows a median reduction in stellar mass of less than 1%. The decreasing importance of AGN feedback in the evolution of small galaxies can be due to the decreasing gas fractions associated with galaxy evolution, a shift in AGN feedback mode from quasar (high redshift) to radio dominated (low redshift), or an evolving black hole population (different M_{SMBH} vs M_* relation) across cosmic time, and we examine each of these options in turn in the following sections.

4.3 The coevolution of SMBHs and their hosts

The maximum feedback energy deposited in the host galaxy is a function of the central SMBH mass squared (see equation 3, using equation 1), so the total effect of AGN feedback will depend directly on the mass of its SMBH. Fig. 6 shows that the median mass of the central black hole undergoes a redshift evolution between $z = 0$ and $z = 5$, with galaxies of a given stellar mass hosting a more massive BH at higher redshift. For example, a galaxy with $M_*^{\text{H-AGN}} = 10^{10} M_\odot$ at redshift $z = 0.5$ typically hosts a SMBH with $M_{\text{SMBH}} = 1.16 \times 10^7 M_\odot$, whereas a galaxy with the same stellar mass at $z = 5$ hosts a SMBH with a median mass of $M_{\text{SMBH}} = 4.2 \times 10^7 M_\odot$. A similar evolution is seen in Merloni et al. (2010) and Decarli et al. (2010).

The evolution of AGN feedback mode with redshift in Fig. 7 reveals that the SMBH population transitions from quasar mode to radio mode between redshifts $z = 3$ and $z = 1$. At high redshift, the vast majority of AGNs are found in quasar mode, namely 95.7% of the sample at $z = 5$ and

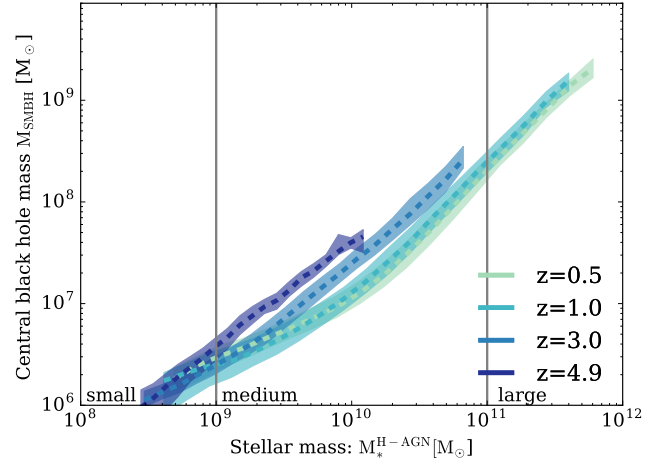


Figure 6. Median black hole mass (dashed lines) evolution as a function of galaxy stellar mass in H-AGN, as well as quartile ranges for the BH mass distribution (shaded region). The plot shows a clear redshift evolution, with smaller galaxies hosting larger black holes at higher redshift³. Note that small galaxies with stellar masses below $M_*^{\text{H-AGN}} < 10^9 M_\odot$ are to be treated with some caution, as they are quite sensitive to resolution effects.

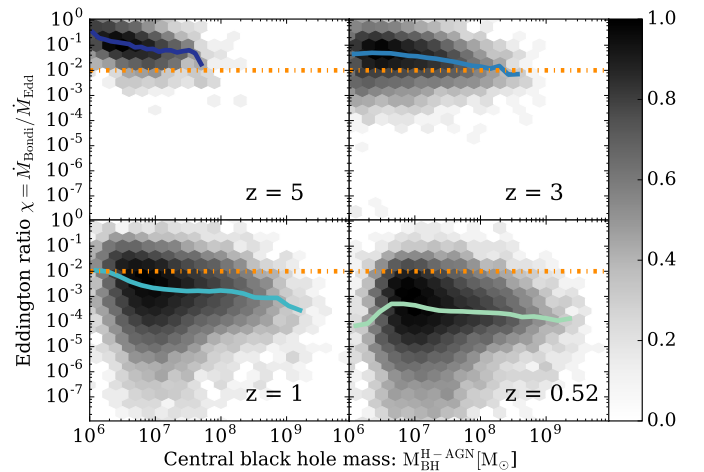


Figure 7. Evolution of AGN feedback mode for the whole sample of SMBHs at different redshifts, with objects above the dotted line in quasar mode and objects below in radio mode. The solid lines denote the median Eddington ratio. There is a clear redshift evolution of the feedback mode, with 95.7% of SMBHs in quasar mode at $z = 5$, in comparison to only 3.8% at $z = 0.5$. The colourbar in each panel is normalised to the bin with the maximum number of objects at the given redshift.

85.5% at $z = 3$. At lower redshift, the population is overwhelmingly in radio mode across all mass bins, with only 19.1% and 3.8% found in quasar mode at $z = 1$ and $z = 0.5$ respectively.

The decrease of the median Eddington ratio with decreasing redshift explains the higher central SMBH masses at higher redshifts, for fixed galaxy stellar masses. While

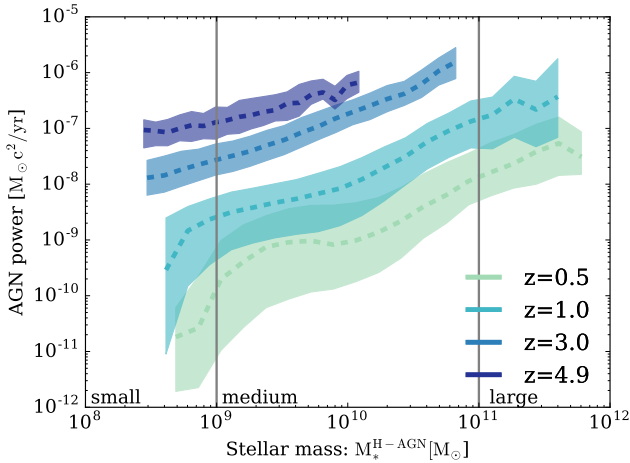


Figure 8. Median AGN power \dot{E}_{AGN} (see equation 3) for each galaxy stellar mass bin in H-AGN, with the shaded region showing the samples quartile error ranges. At higher redshift, a galaxy of the same mass is subject to stronger feedback.

a black hole with $M_{\text{SMBH}} = 10^7 M_{\odot}$ at redshift $z = 5$ accretes with a mean Eddington ratio of $\chi = 6.27 \times 10^{-2}$, a SMBH with the same mass at redshift $z = 0.5$ accretes at only $\chi = 4.12 \times 10^{-4}$ Eddington. This means that the latter grows up to two orders of magnitude more slowly than the former. Moreover, smaller mass black holes at high redshift accrete at a faster relative rate than larger ones, a trend which becomes less pronounced as redshift decreases. These effects respectively drive the redshift evolution of the $M_{*} - M_{\text{SMBH}}$ relation and its flattening, as shown in Fig. 6.

Due to the different radiative efficiencies employed for the two feedback modes, $\epsilon_f = 0.15$ for the quasar mode at $\chi \geq 0.01$ and $\epsilon_f = 1.0$ for the radio mode at $\chi < 0.01$, (see Section 2.5), feedback becomes more effective at redshifts below $z < 2$. However, this effect is not enough to compensate for the decrease in accretion rate, as can be seen in Fig. 8. The consequence of this evolution in accretion rate and central SMBH mass is that, even with the shift in feedback mode around redshift $z = 2$, a galaxy of the same stellar mass is subject to stronger feedback at high redshift. For example, a galaxy with $M_{*}^{\text{H-AGN}} = 10^{10} M_{\odot}$ is subject to feedback of $\dot{E}_{\text{AGN}} = 10^{-6} M_{\odot} c^2/\text{yr}$ at redshift $z = 5$, whereas a galaxy of the same mass is subject to feedback of only $\dot{E}_{\text{AGN}} = 10^{-9} M_{\odot} c^2/\text{yr}$ at redshift $z = 0.5$. The higher feedback energy per unit stellar mass at high redshift means that AGN are much more effective at quenching star formation in the early universe.

Repeating the analysis, but binning in central black hole mass as opposed to galaxy mass, (Fig. 9, in comparison to Fig. 5) yields further evidence that the redshift evolution measured in the quenching fraction as a function of galaxy mass is driven by the evolution of the SMBH population. Independently of redshift, small black holes, with masses $M_{\text{SMBH}} < 10^7 M_{\odot}$, quench their host galaxy by $\approx 10\%$. Intermediate mass black holes, with masses $10^7 \leq M_{\text{SMBH}} \leq 5 \times 10^8$ show a linear relation between M_{SMBH} and quenching fraction, and large black holes with $M_{\text{SMBH}} > 5 \times 10^8 M_{\odot}$

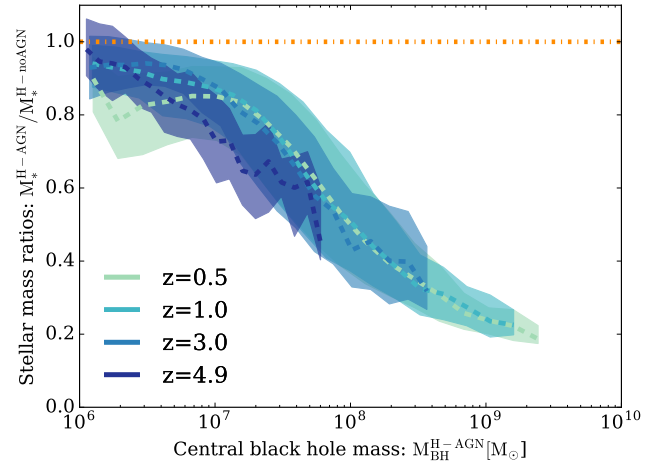


Figure 9. Galaxy mass ratio between H-AGN and H-noAGN versus the mass of the central SMBH of the galaxy, instead of stellar mass as in Fig. 5. The redshift evolution disappears in this case because the feedback energy deposited is directly connected to the central BH mass (see text for detail).

cause the same flattening as can be seen in the plot against stellar mass (see Fig. 5). The evolution in the SMBH population appears to be sufficient to explain the redshift evolution in quenching fraction, with no further dependence on other properties of the host galaxy, which is somewhat surprising. Indeed, if AGN feedback only quenches star formation by driving outflows, one would expect the gas abundance, as well as the depth of the DM potential, to play a role in their effectiveness. However, we found no dependence of the quenching fraction evolution on any of these quantities.³

Although there exists such a clear transition of the sample from one AGN feedback mode to the other, no significant difference was found when analysing the quenching fraction (such as in Fig. 9) by splitting the sample into quasar or radio mode galaxies. All the results shown here can be reproduced by assuming that the entire sample can be found in quasar mode at redshifts $z > 2$, and in radio mode otherwise. The only notable discrepancy between the simulation data and this simplified model is that the scatter is somewhat reduced, which is expected as objects found in the opposite feedback mode to the majority of the population are statistical outliers. However, this analysis is based on an instantaneous measure of feedback mode at a specific redshift,

³ The results presented here are consistent with fig. 10 of Volonteri et al. (2016), which reports no redshift evolution in the $M_{*} - M_{\text{SMBH}}$ relation. This is because the redshift evolution we see is mainly driven by low mass black holes at low redshift, a sample excluded by these authors who apply a cut in host halo mass of $M_{\text{halo}} = 8 \times 10^{10} M_{\odot}$. By comparison, the sample analysed here includes all black holes identified within a host galaxy in halos with $M_{\text{halo}} > 4 \times 10^{10} M_{\odot}$. The second difference between these two pieces of work concerns the statistical analysis chosen: while Volonteri et al. (2016) employ a linear fit as used in observational studies, we present median black hole masses and thus allow for a non-linear correlation between black hole and galaxy stellar masses.

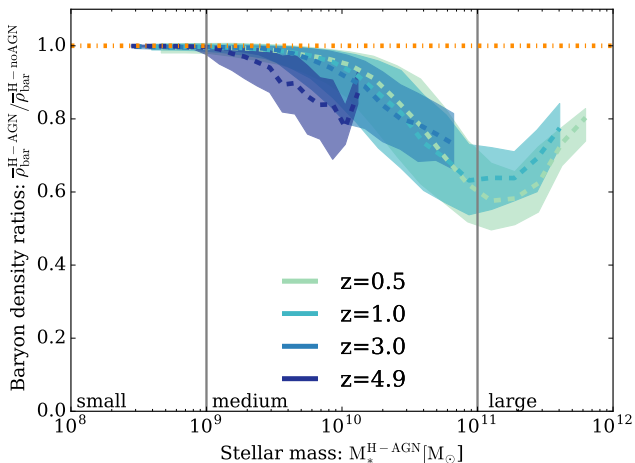


Figure 10. Ratio between the average baryon density $\bar{\rho}_{\text{bar}}^{\text{H-AGN}} / \bar{\rho}_{\text{bar}}^{\text{H-noAGN}}$ within the virial radius of the galaxy host halo twins: $\bar{\rho}_{\text{bar}} = (M_* + M_{\text{SMBH}} + M_{\text{gas}}) / (\frac{4\pi}{3} R_{\text{vir}}^3)$. The dotted line represents identical baryon mass in both host halos, and the shaded regions show the quartile ranges of the sample. AGN feedback partially acts on star formation by reducing the total baryon mass in the halo, particularly for galaxies with stellar masses around $M_*^{\text{H-AGN}} = 10^{11} M_{\odot}$ in H-AGN.

and does not capture the accretion history of a particular object. We defer a more careful analysis of the evolution of the AGN sample, together with an analysis of the timescales on which quenching occurs in individual galaxies, to future work (Beckmann et al 2017, in prep.).

5 AGN FEEDBACK & GAS FLOWS

Fig. 6 shows that SMBHs make up much less than 1% of the mass of their host galaxy, so the mass of baryons accreted by the SMBHs is negligible compared to the reduction in stellar mass caused by quenching. The effect of AGN feedback on the cold gas supply of the galaxy must therefore be profound, to suppress star formation by up to an order of magnitude over the evolution of the galaxy. There are three possible channels through which AGN feedback can affect the gas content of the galaxy: (i) it can drive powerful outflows, emptying the reservoir of gas available in the ISM of the galaxy; (ii) it can prevent cosmic inflows from replenishing the gas supply in the galaxy or (iii) it can heat existing gas of the ISM and circum-galactic medium (CGM) to prevent cooling flows and the associated star formation. In this section, we investigate the relative importance of these three feedback channels.

5.1 The evolution of the baryon content

Should AGN feedback primarily suppress star formation through heating the existing gas in the halo, one would expect twinned halos to have the same total baryon mass, with that in H-AGN showing a much higher gas fraction as less gas is being turned into stars. Fig. 10 shows that AGN feedback directly lowers the baryon (gas + stars + BH) content

embedded within the virial radius of DM halos: the average baryon density ratio versus galaxy stellar mass relation follows a shape reminiscent of that of the quenching fraction previously discussed. Unfortunately all three major channels, through which AGN feedback is expected to affect star formation, lower the baryon density of the galaxy. Boosted outflows drive existing gas out of the galaxy, slowed down inflows prevent accretion in the first place, and heating causes the gas to expand, lowering the average density. We compare the average baryon density, as opposed to the total mass within the halo, to correct for the small differences in halo mass shown in Fig. 4, which translate into a difference in virial radius, and therefore a difference in the volume over which the gas mass in the halo is measured.

Two features stand out in comparison to the quenching fraction. First, the average baryon density within the halo of small galaxies is unaffected by AGN feedback at all redshifts. These galaxies do however show a reduced stellar mass, particularly at redshift $z = 5$, where their stellar mass shows a median reduction of 10%, as seen in Fig. 5. This suggests that feedback affects the star formation efficiency of these galaxies more than it alters their gas supply. Efficiency is reduced either by locally heating the gas, redistributing the gas within the halo, or by destroying dense, star-forming clumps, but not by driving outflows or preventing gas inflows through the halo virial sphere. Secondly, for large galaxies with stellar masses above $M_* > 10^{11} M_{\odot}$, the baryon content in both simulations becomes increasingly comparable again with increasing mass, despite the fact that these galaxies see a reduction in their stellar mass of around 80% for redshifts between $z = 1$ and $z = 0.5$. In this case, the deepening gravitational potential of the halo makes it difficult for the AGN to affect gas flows at the halo virial radius. However a much smaller fraction of the existing gas is converted into stars, because of effects (gas heating / redistribution) similar to those which plague small galaxies. These translate into the significantly reduced galaxy masses presented earlier in Fig. 5. For medium galaxies at all redshifts, AGN feedback acts through depleting the gas reservoir at the halo scale, which reduces the supply of gas available for star formation. This means AGN feedback also directly influence the inflows and/or the outflows of the galaxy. We leave a detailed analysis of the interstellar and intergalactic medium under AGN feedback to future work (Beckmann 2017, in prep.).

5.2 The effect on inflows and outflows

There are two ways to decrease the total baryon mass of a galaxy: by reducing inflows or by boosting outflows. In this work, we measure flows at two different radii: halo scales, also called R95, which correspond to a radius of $R95 = 0.95 \times R_{\text{vir}}$, and galaxy scales, also called R20, which correspond to a radius of $R20 = 0.2 \times R_{\text{vir}}$. Flows are measured through spherical surfaces located at these radii, centred on the halo. Flow masses are calculated for all cells within a narrow shell, centred on the radius in question, where $\dot{M}_{\text{gas}} = \sum_i \rho \Delta x_i^3 \bar{v}_i \cdot \bar{r}_i / \omega$, where ρ is the gas density, Δx is the cell size, \bar{v}_i is the gas velocity, \bar{r}_i is the unit vector of the cell centre relative to the halo centre and $\omega = 2\text{kpc}$ is the width of the shell. M_{outflow} includes all cells with $\bar{v}_i \cdot \bar{r}_i > 0$ and M_{inflow} includes all cells for which $\bar{v}_i \cdot \bar{r}_i \leq 0$.

A first comparative look at the flow patterns for galax-

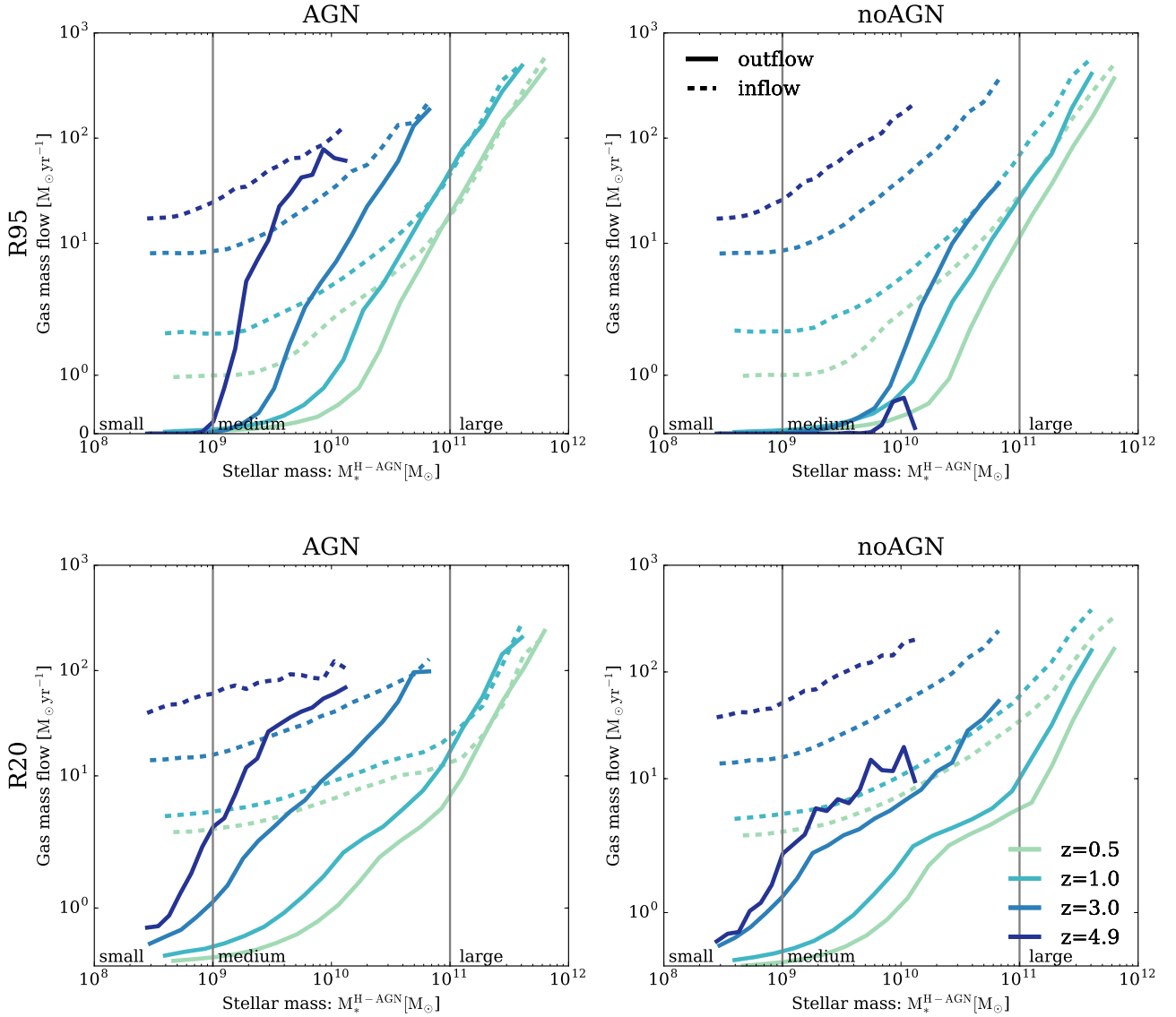


Figure 11. Gas inflows (dashed lines) and outflows (solid lines) at halo (R95, measured at $R = 0.95R_{\text{vir}}$) and galaxy (R20, measured at $R = 0.2R_{\text{vir}}$) scales for both H-AGN and H-noAGN, for a range of redshifts. To simplify the comparison with other plots, flow values for both H-AGN and H-noAGN are plotted against H-AGN galaxy stellar masses. Note that both outflows and inflows represent the median value for a given mass bin, and do not necessarily belong to the same object in H-AGN and H-noAGN. The overall inflows are reduced in the presence of AGN feedback, which also drives outflows at halo scales for medium size galaxies.

ies in H-AGN and H-noAGN (see Fig. 11) suggest that AGN feedback drives outflows in medium and large galaxies, particularly at halo scales. There are also some large scale pseudo flows present for large galaxies. These pseudo flows appear in Fig. 11 because the algorithm used to extract the absolute flow values presented here assumes the halo can be accurately represented by a sphere. However, if the halo is non-spherical, pseudo flows are created. When rotating a non-spherical object through a spherical surface across which absolute mass flows are measured, parts of the object passing out of the sphere will register as outflows, while parts passing in will register as inflows. However, these contributions are not mass flows in the common sense, and cancel out when calculating net mass flows.

Small galaxies undergo no outflows at halo scales, with or without AGN feedback, which matches the conclusion from Fig. 10 that the baryon mass of their halos is identical in H-AGN and H-noAGN. AGN feedback reduces inflows for medium and large galaxies, at both halo and galaxy scales, but the effect is more pronounced at the latter. A more quantitative analysis of the outflows driven by AGN feedback is presented in Fig. 12, where residual flow values for the two simulations are plotted. Residual flows are defined as the mass flow rates in H-AGN relative to those of their twin galaxies in H-noAGN, i.e. $\dot{M}_{\text{gas}}^{\text{residual}} = \dot{M}_{\text{gas}}^{\text{H-AGN}} - \dot{M}_{\text{gas}}^{\text{H-noAGN}}$. This approach has the advantage of isolating the effect of AGN feedback and subtracting out any effects present in both simulations, such as the supernova driven outflows for

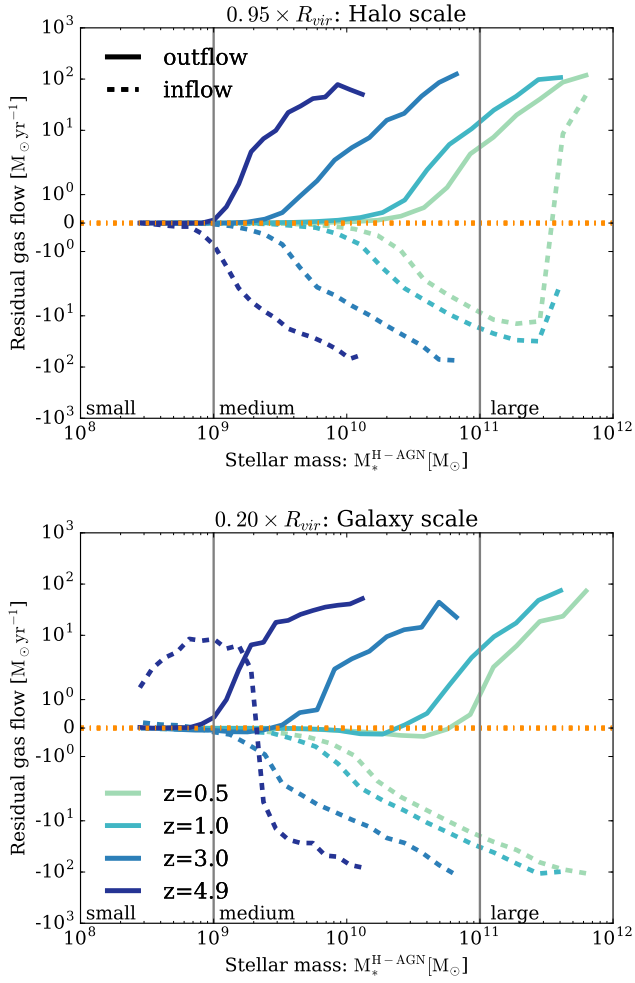


Figure 12. Residual gas flows $\dot{M}_{\text{gas}}^{\text{residual}} = \dot{M}_{\text{gas}}^{\text{H-AGN}} - \dot{M}_{\text{gas}}^{\text{H-noAGN}}$, plotted against the twin’s galaxy stellar mass in H-AGN. Data is presented for flows at two different distances from galaxies, as indicated above each panel, and a range of redshifts. Higher mass flow rates in H-AGN appear above the dash-dotted line, which denotes identical flows in both simulations, and lower mass flow rates sit below this line. Note that both outflows and inflows represent the median value for that mass bin, and do not necessarily belong to the same twin. In general, AGN feedback causes a boost in outflows, and an approximately equal but opposite reduction in inflows.

small and medium galaxies at halo scales, and the pseudo flows seen for large objects at both radii.

The residual gas flows shown in Fig. 12 demonstrate that AGN feedback has an approximately equal and opposite effect on outflows and inflows. Galaxies with stellar masses $M_*^{\text{H-AGN}} \leq 10^{11} M_\odot$ see a similar amount of gas carried away by AGN driven outflows as that depleted in inflows. Apart for small galaxies at high redshift ($z = 5$), where AGN feedback seems able to heat up the gas in the vicinity of the galaxy, causing a gas pile up which triggers larger inflows in H-AGN, the differences between flows at halo and galaxy scales are rather modest. There is a weak trend for boosted outflows to be less dominant at galaxy scales (especially at $z \leq 1$) than at halo scales, and conversely for the suppression

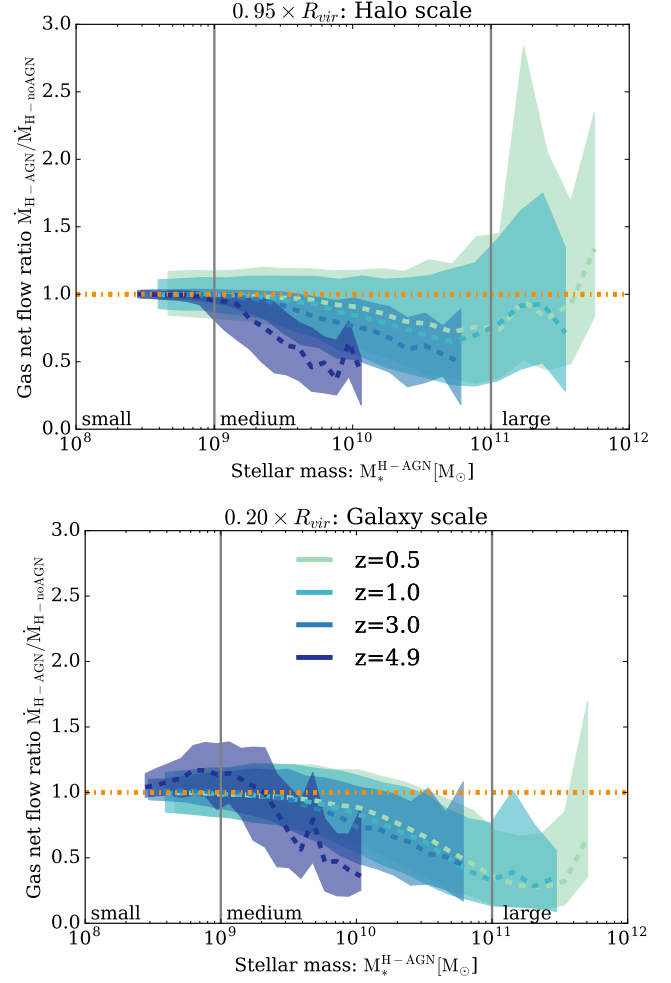


Figure 13. Ratio of net flow rates at halo and galaxy scales as a function of galaxy stellar masses in H-AGN, $M_*^{\text{H-AGN}}$. The dash-dotted horizontal line at a ratio of 1.0 corresponds to identical net flows in both H-AGN and H-noAGN. Data is presented for flows at two different distances from galaxies, as indicated above each panel, and at a range of redshifts. AGN feedback has no effect on flows in small galaxies, produces a reduction in median net flow rates of up to 60% for medium size galaxies, and drives a bursty flow pattern leading to increased net flows at halo scales for large galaxies. Positive net flows are defined to be falling into the object.

of inflows to be more relevant on small scales (especially for galaxies which are less massive than $M_*^{\text{H-AGN}} \leq 10^{10} M_\odot$), but overall material is neither being significantly swept up in the halo and kicked out, nor preferentially deposited there. Rather, these two effects combine to reduce the net median inflow for medium galaxies into both the halo and the galaxy by up to 60% for the most massive objects, as the direct comparison of net inflows for twins in Fig. 13 shows. This results in the reduction in baryon mass seen for the same galaxies in Fig. 10. In agreement with the same figure, small galaxies show no change in net flows at halo scales, which matches their identical baryon mass in the presence and absence of AGN feedback.

For large galaxies, the situation is different, particularly

at low redshift. At halo scales, the simulation with AGN feedback actually shows boosted inflows carrying an amount of mass similar to that in boosted outflows. This means the outflows are being recycled, as AGN feedback becomes unable to gravitationally unbind the gas from the halo. It is important to note that the values plotted here represent the median value for a given mass bin, so the outflow and inflow values do not necessarily belong to the same object. It is therefore not necessarily correct that the two curves cancel out to produce no change in the net flow. Indeed, a comparative analysis of net inflows for each twin across H-AGN and H-noAGN (Fig. 13) shows that at halo scales, the overall inflow is boosted by up to 50% for the most massive galaxies in the presence of AGN feedback.

At galaxy scales, the gas flow patterns for the most massive objects ($M_*^{\text{H-AGN}} > 2 \times 10^{11} M_\odot$ at $z = 0.5$) become harder to predict. In these galaxies, AGNs fall into maintenance feedback mode (see Section 4.3) at redshifts below the peak of star formation, $z = 2$. This produces very bursty outflows, as SMBHs go through cycles of being fed, which triggers strong feedback episodes. The latter drive out the gas, starving the black hole, and the feedback abates until enough gas becomes available again for the SMBH to go through another accretion event. These cycles take place on timescales much shorter than the time interval between the redshift outputs we are considering in this work. Furthermore, the number of such galaxies is quite limited (≈ 1000). We illustrate the impact this has on our results in Fig. 14, which shows that at redshift $z = 0.5$, the median outflow depends quite sensitively on the exact point in time at which the distribution of galaxies is sampled. As the SMBHs cycle rapidly through a wide variety of active and quiescent states, the distribution of residual outflows spans several orders of magnitude. In comparison, the outflows produced by the larger population of smaller galaxies are more steady on similar timescales, and therefore their sampling is more robust (see left panel of Fig. 14). We would like to point out that the variation timescales of the large scale outflows studied here do not necessarily reflect the duty cycle of the SMBH, as each burst can be driven by a series of feedback events. We postpone a more detailed analysis of the SMBH duty cycles in the simulation to future work (Beckmann 2017 et al, in prep).

It is interesting to note that the lack of excess outflows for low mass galaxies ($M_*^{\text{H-AGN}} < 5 \times 10^{10} M_\odot$ at $z = 0.5$) in Fig. 12 does not mean that the outflows for any given matching galaxy pair in H-AGN and H-noAGN are identical. As the panel on small galaxies in Fig. 14 demonstrates, individual objects show a variety of residual outflows (and inflows). The build-up of small differences in galaxy properties not necessarily induced by AGN feedback (e.g. stochastic star formation algorithm, seeding and growth of the central SMBH) can result in temporarily diverging residual outflow histories at low redshift. In other words, even though the precise amount of residual outflow from any specific twinned pair of galaxies does depend on the timescale of the outflow and so is sensitive to the redshift at which it is measured, the lack of any marked systematic difference in the gas flow pattern due to AGN feedback registers as a median residual outflow of zero for the whole sample.

Another note of caution concerns the residual flows in Fig. 12, which likely underestimate the effect of AGN on

inflows and outflows. Particularly for massive galaxies at low redshift, where the H-noAGN twin has a stellar mass $\sim 5 \times$ that of the H-AGN one, the H-noAGN twin has stronger stellar flows that obscure some of the AGN driven effects when calculating residual gas flows as $\dot{M}_{\text{gas}}^{\text{residual}} = \dot{M}_{\text{gas}}^{\text{H-AGN}} - \dot{M}_{\text{gas}}^{\text{H-noAGN}}$. Finally, we come back to the asymmetry between residual inflows and outflows with respect to the zero residual line, which is stronger at galaxy than halo scales. In light of the previous remarks about outflow timescales, we can safely attribute this difference as meaning that AGN feedback does preferentially suppress inflows in the vicinity of all galaxies rather than eject gas from them, except perhaps at the very high mass end of the galaxy stellar mass function, $M_*^{\text{H-AGN}} > 3 \times 10^{11} M_\odot$ at low redshifts ($z < 0.5$).

Overall, flow patterns due to AGN feedback, made up in roughly equal parts of boosted outflows and reduced inflows at halo scales, comfortably explain the non-linear distribution of baryon masses plotted in Fig. 10, which combines with a reduced star formation efficiency across all galaxy mass bins to produce the quenching fractions shown in Fig. 5.

6 CONCLUSIONS

We have isolated the effect of AGN feedback on stellar quenching in massive galaxies by comparing two cosmological simulations, H-AGN and H-noAGN, which were run with and without AGN feedback respectively. More specifically, by twinning individual DM halos and galaxies across the two simulations, we have been able to quantify the effect of feedback on individual objects throughout cosmic time. In agreement with a large body of previous work (such as (such as Springel et al. 2005; Bower et al. 2006; Sijacki et al. 2007; Ciotti & Ostriker 2007; Cattaneo & Teyssier 2007; Dubois et al. 2013; Gene et al. 2014; Schaye et al. 2014; Pontzen et al. 2017, , among others), among others) our results show that AGN feedback is instrumental in quenching the massive end of the GSMF. Whilst the stellar mass of galaxies without AGN feedback closely follows predictions based on the assumption that all baryons contained in dark matter halos end up forming stars, galaxies subject to the influence of AGN feedback end up with masses distributed according to a GSMF that shows a characteristic exponential steepening at the high mass end, in line with observations (Bielby et al. 2014; Daddi et al. 2002; Moustakas et al. 2013; Tomczak et al. 2014; González et al. 2011; Song et al. 2016).

However, a closer comparison of the stellar mass for individual objects reveals a non-linear dependence of quenching fraction on mass, with the most massive galaxies being the most strongly quenched, and the smallest galaxies mostly unaffected by AGN feedback. This leads to a characteristic shape for the mass ratio $M_*^{\text{H-AGN}}/M_*^{\text{H-noAGN}}$, which shows a linear dependence on $\log(M_*^{\text{H-AGN}})$, the stellar mass of the galaxy in H-AGN, for medium sized galaxies with $10^9 M_\odot \lesssim M_*^{\text{H-AGN}} \lesssim 10^{11} M_\odot$ (the exact values depend on redshift), but tails off at both low and high mass ends. The most massive galaxies, with $M_* > 10^{11} M_\odot$ are most strongly quenched and contain only 20% of the stellar mass in the presence of AGN feedback, in comparison to the case without feedback.

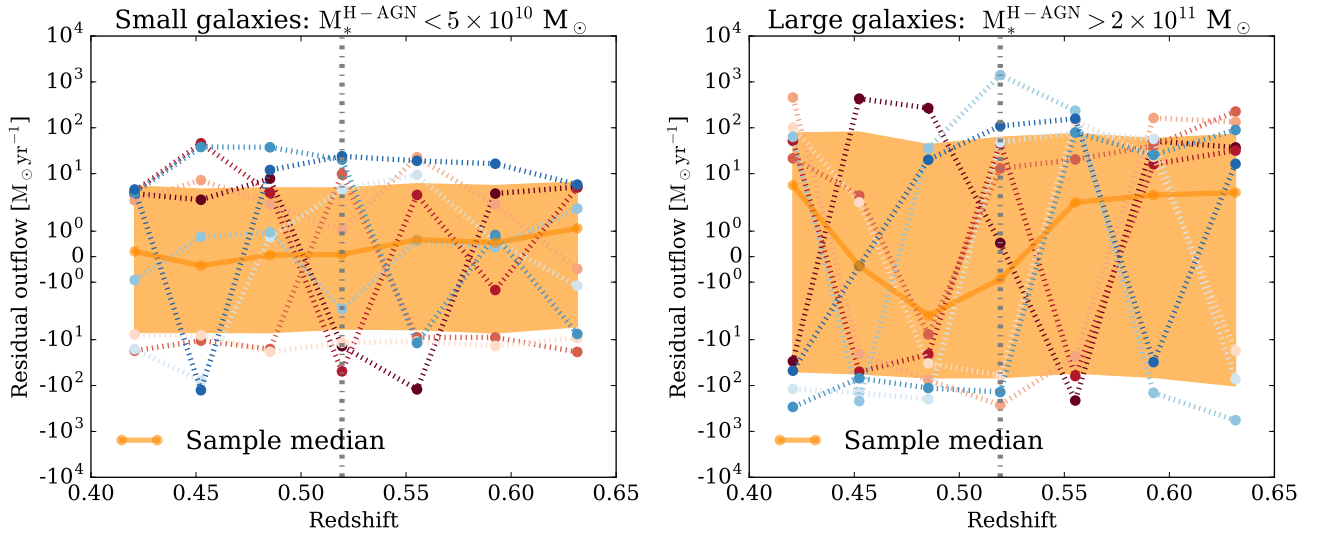


Figure 14. Residual outflows due to AGN feedback at galaxy scales, $R_{20} = 0.2 \times R_{\text{vir}}$, plotted for 10 randomly selected galaxies within the small and large galaxy mass bins, between redshifts $0.64 > z > 0.42$. The solid line represents the median sample output, with the shaded region covering quartile error ranges. The vertical dotted line represents redshift $z = 0.52$, for comparison with Fig. 12. This shows that outflows from large galaxies (right panel) with stellar masses $M_*^{\text{H-AGN}} > 2 \times 10^{11} M_\odot$ at redshifts around $z = 0.52$ (dotted vertical line) vary on very short timescales, so the median outflow value, (solid line, with quartile error ranges represented by the shaded regions), is very sensitive to the exact time at which it is sampled. By comparison, the outflows for small galaxies with stellar masses $M_*^{\text{H-AGN}} < 5 \times 10^{10} M_\odot$ (left panel) vary much less on these timescales, and the median value is less sensitive to variations in time.

We also find a significant redshift evolution for the smallest galaxy mass to be affected by AGN feedback, with smaller galaxies being more quenched at higher redshift. This evolution is caused by the median central black hole mass of galaxies increasing with redshift by up to an order of magnitude. This combines with higher accretion rates at high redshift, due to gas-rich galaxies, such that a galaxy of the same stellar mass is subject to AGN feedback up to three orders of magnitude stronger at redshift $z = 5$ than at $z = 0.5$. We also measure a shift in feedback mode, with at least 85.5% of AGN at redshift $z = 3$ and above in quasar mode, compared with a maximum of 19.1% at lower redshifts. Overall we find galaxy stellar mass quenching to be a continuous process active throughout the entire evolution of the galaxy.

A comparative analysis of the baryon content of halos reveals that AGN feedback quenches star formation through a combination of reducing the total gas supply within the halo by driving outflows, and preventing accretion of fresh gas by curbing inflows. Small galaxies with $M_*^{\text{H-AGN}} \leq 10^9 M_\odot$ show nearly identical baryon masses with and without AGN feedback, as the flows at halo-scales remain chiefly unaffected by feedback. Note that this is not true at galaxy scales and high redshift, where gas inflows can be somewhat enhanced by feedback for these small objects. On the other hand, medium size galaxies $10^9 M_\odot \leq M_*^{\text{H-AGN}} \leq 10^{11} M_\odot$ experience a significant reduction in baryon mass, caused by an approximately equal contribution from AGN-driven gas outflows and a reduction of cosmic inflows. At galaxy scales, the reduction of inflows dominates. Finally, for large galaxies ($10^{11} M_\odot \leq M_*^{\text{H-AGN}}$) the baryon mass rises again, as inflows at halo scales are swelled by gas expelled by AGN

feedback in the inner regions, which remains gravitationally bound and falls back into the halo. At galaxy scales, outflows for the most massive objects vary on very short timescales, as the AGN enter a bursty maintenance mode. Thus the gas mass has a tendency to increase on average (as compared to medium size galaxies), even though the stellar mass does not, given the long characteristic timescale of star formation.

Overall, we conclude that AGN feedback effectively quenches the massive end of the galaxy mass function over the entire evolution of the galaxy population. AGN feedback acts by reducing the stellar content of galaxies by up to 80% (for the most massive objects) through a mixture of increased outflows and reduced inflows, combined with a decreased star formation efficiency of in situ gas. We predict that the influence of AGN feedback should already be noticeable by redshift $z = 5$, for galaxies with relatively modest stellar masses ($M_* \approx 10^{10} M_\odot$) by current epoch standards, as these objects are close to the top end of the GSMF at these redshifts. This is exciting news as the James Webb Space Telescope should be able to test this prediction in the near future.

ACKNOWLEDGEMENTS

This work used the HPC resources of CINES (Jade supercomputer) under the allocation 2013047012 made by GENCI, and the horizon and Dirac clusters for post processing. This work is partially supported by the Spin(e) grants ANR-13-BS05-0002 of the French Agence Nationale de la Recherche and by the National Science Foundation under Grant No. NSF PHY11- 25915, and it is part of the Horizon-

UK project, so part of the analysis of the H-AGN and H-noAGN simulations was performed on the DiRAC Facility jointly funded by BIS and STFC. The research of RB is supported by STFC, and the research of AS, MLAR and JD at Oxford is supported by the Oxford Martin School and Adrian Beecroft. NC is supported by a Beecroft postdoctoral fellowship.

REFERENCES

- Arav N., et al., 2001, *ApJ*, 561, 118
- Barro G., et al., 2016, *ApJ*, 820, 120
- Benson A. J., Bower R. G., Frenk C. S., Lacey C. G., Baugh C. M., Cole S., 2003, *ApJ*, 599, 38
- Bernardi M., Meert A., Sheth R. K., Vikram V., Huertas-Company M., Mei S., Shankar F., 2013, *MNRAS*, 436, 697
- Bielby R. M., et al., 2014, *A&A*, 568, A24
- Bieri R., Dubois Y., Silk J., Mamon G. A., 2015, *ApJ*, 812, L36
- Binney J., Tabor G., 1995, *MNRAS*, 276, 663
- Booth C. M., Schaye J., 2009, *MNRAS*, 398, 53
- Bower R. G., Benson A. J., Malbon R., Helly J. C., Frenk C. S., Baugh C. M., Cole S., Lacey C. G., 2006, *MNRAS*, 370, 645
- Cattaneo A., 2001, *MNRAS*, 324, 128
- Cattaneo A., Teyssier R., 2007, *MNRAS*, 376, 1547
- Cattaneo A., et al., 2009, *Nature*, 460, 213
- Chartas G., Brandt W. N., Gallagher S. C., Proga D., 2007, *AJ*, 133, 1849
- Christensen C. R., Davé R., Governato F., Pontzen A., Brooks A., Munshi F., Quinn T., Wadsley J., 2016, *ApJ*, 824, 57
- Cicone C., et al., 2014, *A&A*, 562, A21
- Ciotti L., Ostriker J. P., 2007, *ApJ*, 665, 1038
- Cole S., Aragon-Salamanca A., Frenk C. S., Navarro J. F., Zepf S. E., 1994, *MNRAS*, 271, 781
- Costa T., Sijacki D., Haehnelt M. G., 2015, *MNRAS*, 448, L30
- Croton D. J., et al., 2006, *MNRAS*, 365, 11
- Daddi E., et al., 2002, *A&A*, 384, L1
- Davidzon I., et al., 2017, arXiv Prepr.
- De Kool M., Arav N., Becker R. H., Gregg M. D., White R. L., Laurent-Århem Muehleisen S. A., Price T., Korista K. T., 2001, *ApJ*, 548, 609
- Decarli R., Falomo R., Treves A., Labita M., Kotilainen J. K., Scarpa R., 2010, *MNRAS*, 402, 2453
- Dekel A., Burkert A., 2014, *MNRAS*, 438, 1870
- Dekel a., Silk J., 1986, *ApJ*, 303, 39
- Di Matteo T., Springel V., Hernquist L. E., 2005, *Nature*, 433, 604
- Di Matteo T., Colberg J., Springel V., Hernquist L., Sijacki D., 2008, *ApJ*, 676, 33
- Dubois Y., Teyssier R., 2008, *A&A*, 477, 79
- Dubois Y., Devriendt J., Slyz A., Teyssier R., 2010, *MNRAS*, 409, 985
- Dubois Y., Devriendt J., Slyz A., Teyssier R., 2012, *MNRAS*, 420, 2662
- Dubois Y., Pichon C., Devriendt J., Silk J., Haehnelt M., Kimm T., Slyz A., 2013, *MNRAS*, 428, 2885
- Dubois Y., et al., 2014, *MNRAS*, 444, 1453
- Dubois Y., Volonteri M., Silk J., Devriendt J., Slyz A., Teyssier R., 2015, *MNRAS*, 452, 1502
- Dunn J. P., et al., 2010, *ApJ*, 709, 611
- Efstathiou G., 2000, *MNRAS*, 317, 697
- Fabian A., 2012, *ARA&A*, 50, 455
- Fabian A. C., Celotti A., Erlund M. C., 2006, *MNRAS*, 373, L16
- Farrah D., et al., 2012, *ApJ*, 745, 178
- Feldmann R., Mayer L., 2014, *MNRAS*, 446, 1939
- Ferrarese L., Merritt D., 2000, *ApJ*, 539, L9
- Franx M., van Dokkum P. G., Förster Schreiber N. M., Wuyts S., Labbé I., Toft S., 2008, *ApJ*, 688, 770
- Gaibler V., Khochfar S., Krause M., Silk J., 2012, *MNRAS*, 425, 438
- Gebhardt K., et al., 2000, *ApJ*, 539, L13
- Geen S., Slyz A., Devriendt J., 2013, *MNRAS*, 429, 633
- Gene S., et al., 2014, *MNRAS*, 445, 175
- Girardi L., Bressan A., Bertelli G., Chiosi C., 2000, *A&AS*, 141, 371
- Gnedin N. Y., 2000, *ApJ*, 542, 535
- González V., Labbé I., Bouwens R. J., Illingworth G., Franx M., Kriek M., 2011, *ApJ*, 735, L34
- Governato F., Willman B., Mayer L., Brooks A., Stinson G., Valenzuela O., Wadsley J., Quinn T., 2007, *MNRAS*, 374, 1479
- Haardt F., Madau P., 1996, *ApJ*, 461, 20
- Habouzit M., Volonteri M., Latif M., Dubois Y., Peirani S., 2016, *MNRAS*, 463, 529
- Heckman T. M., Kauffmann G., 2006, *New Astron.*, 50, 677
- Heckman T. M., Lehnert M. D., Strickland D. K., Armus L., 2000, *ApJ*, 129, 493
- Hopkins P. F., Keres D., Onorbe J., Faucher-Giguere C.-A., Quataert E., Murray N., Bullock J. S., 2014, *MNRAS*, 445, 581
- Kauffmann G., White S. D. M., Guiderdoni B., 1993, *MNRAS*, 264, 201
- Kaviraj S., et al., 2016, arXiv Prepr., 000
- Keller B. W., Wadsley J., Couchman H. M. P., 2015, *MNRAS*, 453, 3500
- Kennicutt, Jr. R. C., 1998, *ApJ*, 498, 541
- Kimm T., Cen R., Devriendt J., Dubois Y., Slyz A., 2015, *MNRAS*, 451, 2900
- Komatsu E., et al., 2011, *ApJS*, 192, 18
- Krumholz M. R., Tan J. C., 2007, *ApJ*, 654, 304
- Leitherer C., Robert C., Drissen L., 1992, *ApJ*, 401, 596
- Leitherer C., et al., 1999, *ApJS*, 123, 3
- Leitherer C., Ortiz Otálvaro P. A., Bresolin F., Kudritzki R.-P., Lo Faro B., Pauldrach A. W. A., Pettini M., Rix S. A., 2010, *ApJS*, 189, 309
- Lutz D., et al., 2008, *ApJ*, 684, 853
- Mac Low M.-M., Ferrara A., 1999, *ApJ*, 513, 142
- Maiolino R., et al., 2012, *MNRAS*, 425, 66
- Mandelbaum R., Wang W., Zu Y., White S., Henriques B., More S., 2016, *MNRAS*, 457, 3200
- Matteucci F., Greggio L., 1986, *A&A*, 154, 279
- Merloni A., et al., 2010, *ApJ*, 708, 137
- Moe M., Arav N., Bautista M. A., Korista K. T., 2009, *ApJ*, 706, 525
- Moustakas J., et al., 2013, *ApJ*, 767, 50
- Murray N., Quataert E., Thompson T. a., 2005, *ApJ*, 618, 569
- Nardini E., Risaliti G., Salvati M., Sani E., Imanishi M., Marconi A., Maiolino R., 2008, *MNRAS*, 385
- Nomoto K., Saio H., Kato M., Hachisu I., 2007, *ApJ*, 663, 1269
- Okamoto T., Gao L., Theuns T., 2008, *MNRAS*, 390, 920
- Omma H., Binney J., Bryan G., Slyz A., 2004, *MNRAS*, 348, 1105
- Page M. J., et al., 2012, *Nature*, 485, 213
- Peirani S., et al., 2016, arXiv Prepr., p. 18
- Pontzen A., Tremmel M., Roth N., Peiris H. V., Saintonge A., Volonteri M., Quinn T., Governato F., 2017, *MNRAS*, 465, 547
- Prunet S., Pichon C., Aubert D., Pogosyan D., Teyssier R., Gottloeber S., 2008, *ApJS*, 178, 179
- Quintero A. D., et al., 2004, *ApJ*, 602, 190
- Rafferty D. A., McNamara B. R., Nulsen P. E. J., Wise M. W., 2006, *ApJ*, 652, 216
- Rasera Y., Teyssier R., 2006, *A&A*, 445, 1
- Reeves J. N., O'Brien P. T., Ward M. J., 2003, *ApJ*, 593, L65

- Rosdahl J., Schaye J., Dubois Y., Kimm T., Teyssier R., 2017, *MNRAS*, 466, 11
- Saez C., Chartas G., Brandt W. N., 2009, *ApJ*, 697, 194
- Salpeter E. E., 1954, *ApJ*, 121, 161
- Santini P., et al., 2012, *A&A*, 540, A109
- Schawinski K., et al., 2014, *MNRAS*, 440, 889
- Schaye J., et al., 2014, *MNRAS*, 446, 521
- Shakura N. I., Sunyaev R. a., 1973, *A&A*, 24, 337
- Sijacki D., Springel V., Di Matteo T., Hernquist L., 2007, *MNRAS*, 380, 877
- Sijacki D., Vogelsberger M., Genel S., Springel V., Torrey P., Snyder G. F., Nelson D., Hernquist L., 2015, *MNRAS*, 452, 575
- Silk J., 2005, *MNRAS*, 364, 1337
- Somerville R. S., 2002, *ApJ*, 572, L23
- Song M., et al., 2016, *ApJ*, 825, 5
- Springel V., Di Matteo T., Hernquist L., 2005, *MNRAS*, 361, 776
- Sturm E., et al., 2011, *ApJ*, 733, L16
- Sutherland R. S., Dopita M. A., 1993, *ApJS*, 88, 253
- Teyssier R., 2002, *A&A*, 385, 337
- Thomas D., Thomas D., Maraston C., Maraston C., Bender R., Bender R., de Oliveira C. M., de Oliveira C. M., 2005, *ApJ*, 621, 673
- Tomczak A. R., et al., 2014, *ApJ*, 783, 85
- Tomczak A. R., et al., 2016, *ApJ*, 817, 118
- Tremonti C. a., Moustakas J., Diamond-Stanic A. M., 2007, *ApJ*, 663, L77
- Vassiliadis E., Wood P. R., 1993, *ApJ*, 413, 641
- Veilleux S., Cecil G., Bland-Hawthorn J., 2005, *ARA&A*, 43, 769
- Volonteri M., Dubois Y., Pichon C., Devriendt J., 2016, *MNRAS*, 460, 2979
- Weiner B. J., et al., 2009, *ApJ*, 692, 187
- White S. D. M., Frenk C. S., 1991, *ApJ*, 379, 52
- Williams R. J., Maiolino R., Krongold Y., Carniani S., Cresci G., Mannucci F., Marconi A., 2016, arXiv Prepr.
- Zolotov A., et al., 2015, *MNRAS*, 450, 2327

This paper has been typeset from a $\text{\TeX}/\text{\LaTeX}$ file prepared by the author.